Apparent birefringence in critical-angle refractometry: a polarization bias of the derivative method

Ierotheos Katsoulis · draft of Nov 4, 2026

Self-published preprint, not peer-reviewed. Text and figures © 2026 Ierotheos Katsoulis, licensed CC BY 4.0; analysis code MIT-licensed. Measurements were made at the Electronic Devices and Materials Laboratory (EDML), Department of Electrical and Electronic Engineering, University of West Attica, during an MSc by Research supervised by Prof. Konstantinos Moutzouris (2020–2021). The full measurement dataset may be the property of EDML, UNIWA and is not disclosed; a representative sample is provided for verification and is not covered by the CC BY license. *Cite as:* I. Katsoulis, "Apparent birefringence in critical-angle refractometry: a polarization bias of the derivative method," self-published preprint, November 2026.

Abstract

The derivative method of critical-angle refractometry makes an isotropic liquid look birefringent: for water it reports $n_{TM} - n_{TE} = +(6.6 \pm 0.6) \times 10^{-5}$ although the true value is zero.

The artefact arises because the TE and TM reflectance edges have different shapes. Anything that rounds the edge — discrete angular sampling and smoothing, the instrument's angular spread, or sample absorption — moves the TE derivative maximum further below the critical angle than the TM one. We measured 252 TE and TM profiles of water at 532, 633, 964 and 1551 nm with a commercial prism coupler. A forward model, constrained only by the measured widths, asymmetries and edge reflectances of the derivative peaks, predicts the artefact at each wavelength with no parameter fitted to the indices. Subtracting it leaves $n_{TM} - n_{TE} = (-0.04 \pm 0.91) \times 10^{-5}$.

The artefact grows with the angular spread σ, is proportional to $(n_p/n)^2 - 1$, and reaches about 10^{-4} for low-index samples on high-index prisms. That is comparable to the stated index resolution of commercial instruments. The angular spread found here, 0.24–0.44 mrad, is usually assumed to be negligible. Yet if the 1551 nm TE/TM difference were attributed to absorption, the inferred extinction coefficient would be 6.4 times too large. We also report a 9×10^{-4} index offset between the two directions of table rotation, and give a correction procedure and measurement protocol.

1. Introduction

The errors of the derivative method studied so far come from the sample; this paper shows that the instrument and the analysis add a polarization-dependent error of the same size.

In critical-angle refractometry a sample is placed on a prism of index n_p and the internal reflectance $R(\theta)$ is scanned through the critical angle [1]. The derivative method takes the maximum of $dR/d\theta$ as θ_c and returns $n = n_p \sin \theta_c$ [4]. Commercial prism couplers use it to measure bulk and thick-film indices with a stated resolution of $\pm 1 \times 10^{-4}$. They measure in-plane and out-of-plane birefringence by repeating the scan in TE and TM polarization [13], extending the prism-coupler birefringence methods for thin films [12].

For absorbing samples the derivative maximum lies below the true critical angle. Meeten and co-workers computed the resulting index errors from the Fresnel equations [2, 3], and these errors have since been studied for turbid colloids [11], absorbing liquids [10] and critical-angle sensor design [9]. Koutsoumpos et al. turned the error into information. The extended derivative method retrieves n and k from the angle and reflectance at the derivative maximum [5]; variants use a known k [6], two prisms [7], or the s- and p-polarized critical angles of an isotropic medium [8]. These analyses assume an ideally collimated beam. The two-prism study states the common assumption explicitly: the uncertainty in θ_c is set by the step of the rotary table, 0.001–0.005°, and is practically insensitive to the divergence of the laser beam [7].

We test that assumption with liquid water, a sample known to be optically isotropic. Any difference between its TE and TM indices must be an artefact. We show that the measured difference is significant, that its size follows from the measured shapes of the derivative peaks, and that it is dominated by angular sampling and spread rather than by absorption. To our knowledge, the polarization dependence of this instrumental error has not been quantified before. Finite-beam effects near the critical angle are known to differ between polarizations (for example the Goos–Hänchen shift [20]), but they have not been related to the derivative-method index.

2. Origin of the bias

The TE and TM reflectances share the same critical angle but approach it with different slopes, so any rounding of the edge shifts their derivative maxima by different amounts.

With $\varepsilon = (n/n_p)^2$ and $w = (\varepsilon - \sin^2\theta)^{1/2}$ ($\mathrm{Im}\, w \geq 0$), the internal Fresnel coefficients are [18]

$$r_{\mathrm{TE}} = \frac{\cos\theta - w}{\cos\theta + w}, \qquad r_{\mathrm{TM}} = \frac{\varepsilon\cos\theta - w}{\varepsilon\cos\theta + w}$$

For a transparent sample, just below θ_c ($\delta = \theta_c - \theta \to 0$)

$$1 - R_{\mathrm{TE}} \simeq \frac{4}{\cos\theta_c}\sqrt{\delta \sin 2\theta_c}, \qquad 1 - R_{\mathrm{TM}} \simeq \frac{1}{\varepsilon}\left(1 - R_{\mathrm{TE}}\right)$$

The TM edge is $1/\varepsilon$ times steeper: about 2.2 times for water on an $n_p \approx 1.96$ prism. Further from θ_c the square-root law fails earlier for TM, so the two profiles differ in shape, not only in scale (Fig. 1). Three processes round the edge:

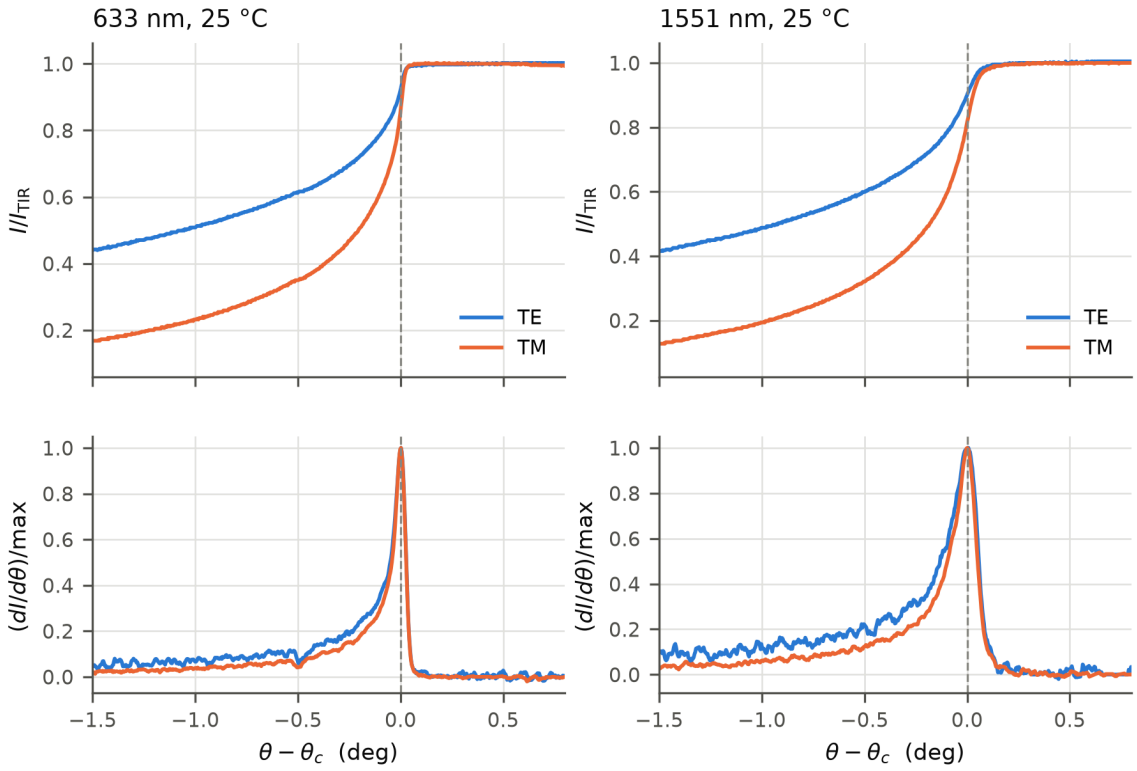


Fig. 1. Measured TE and TM profiles of water at 25 °C (top: intensity normalized to the total-reflection level; bottom: smoothed derivative), plotted against the angle from the derivative maximum. The TE edge carries more weight below θ_c, so its derivative peak is wider.

1. **Sampling and smoothing.** The profile is sampled every Δθ and differentiated with a smoothing filter of finite width.
2. **Angular spread.** Beam divergence, spot size and detector aperture average R(θ) over a distribution of width σ.
3. **Absorption.** With k > 0 the singularity at θ_c disappears [2, 3, 5].

Each pulls the derivative maximum below θ_c, and the pull is larger for TE. The derivative method therefore underestimates n in both polarizations, and underestimates it more in TE, which produces an apparent $n_{TM} > n_{TE}$.

Simulations (Section 4) show that for a transparent sample the artefact separates into an instrument factor and an index factor:

$$\Delta_{\mathrm{TM}} - \Delta_{\mathrm{TE}} \approx C(\sigma, \Delta\theta, w_{\mathrm{SG}}) \left[\left(\frac{n_p}{n} \right)^2 - 1 \right]$$

The factor $(n_p/n)^2 - 1 = 1/\varepsilon - 1$ measures how unlike the two edges are. For 0.0036° sampling and a 15-point Savitzky–Golay filter, C = 1.6, 3.1 and 6.6 × 10^{-5} at σ = 0, 0.02 and 0.04°. This holds within about 10 % for n/n_p from 0.60 to 0.84 (Fig. 2a). The artefact is largest for low-index samples on high-index prisms, which is exactly the configuration used for liquids and polymers.

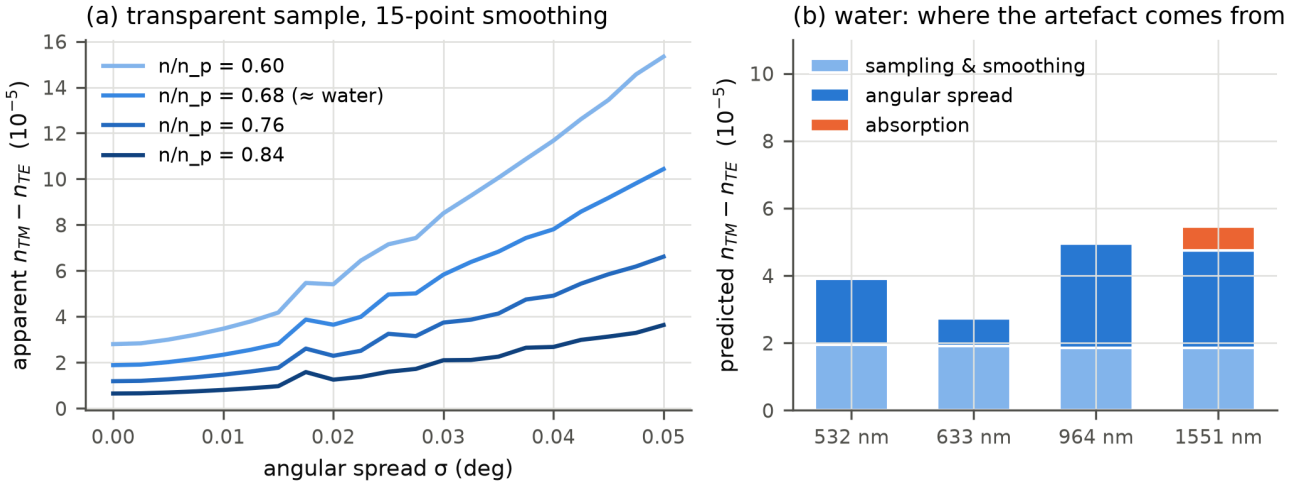


Fig. 2. (a) Apparent $n_{TM} - n_{TE}$ of a transparent sample versus angular spread, for four sample/prism index ratios (0.0036° sampling, 15-point smoothing). Small steps come from the discrete angular sampling. (b) Predicted artefact for water at 25 °C, split into sampling and smoothing (σ = 0, k = 0), angular spread (the inferred σ) and absorption (literature k).

3. Test sample and measurements

Water is a good test sample because its bulk isotropy is guaranteed by symmetry, and its index is tabulated to about 10^{-4} in the visible and its absorption is well known [14–17]. Its absorption also spans four orders of magnitude across the near infrared, from k ≈ 10^{-8} at 633 nm to 1.3 × 10^{-4} at 1551 nm [16, 17], which separates the instrumental and absorption contributions.

All 252 scans were taken with a Metricon 2010/M prism coupler [13] (prism indices 1.9775, 1.9642, 1.9450 and 1.9340 at 532, 633, 964 and 1551 nm; laser power ≈ 0.8 mW) in October–November 2020. A cell with an opening in its base held water for injection against the prism. Each scan covers about 39–45° of internal angle in steps of 0.0036°. The prism was held at 25 or 70 °C (plus short runs at 50 and 80 °C).

The polarization was set by a computer-controlled polarizer. Before each polarization series the cell was emptied, refilled and re-clamped, and the instrument was re-referenced. Within a series, consecutive scans

alternate between the two directions of table rotation (L and R). Each wavelength, temperature, polarization and direction has 1 to 15 scans; most of the 25 °C groups have 9–15.

4. Forward model and inference

The correction uses only quantities that the data already contain: the shapes of the derivative peaks fix the instrument's angular spread, and that spread predicts the TE and TM biases.

Data reduction. Isolated spikes are replaced by a running median. Each scan is differentiated with a 15-point quadratic Savitzky–Golay filter [19], and the maximum is refined by a parabola, giving θ_c and $n_{SDM} = n_p \sin \theta_c$. We also record three shape observables: the full width at half maximum of the derivative peak, its asymmetry, and the edge reflectance $R_c = I(\theta_c)/I_{TIR}$. L and R scans are averaged separately and combined as $(n_L + n_R)/2$.

Model. Synthetic scans are generated as

$$I(\theta) = A\left[R_{\mathrm{pol}}(\,\cdot\,; n, k) * g_\sigma\right](\theta) + B$$

with g_σ a Gaussian of standard deviation σ, sampled at the measured angular step and passed through exactly the same reduction code. The derivative-method result is invariant to A and B, so the bias $\Delta_{pol} = n_{SDM} - n$ depends only on σ, k, n/n_p and the analysis settings.

Inference. For each wavelength and temperature we evaluate a grid of σ (0.004–0.070°) and $\log_{10}$ k (−9 to −3). Each grid point is scored by a χ^2 on the six shape observables (three per polarization), weighted by their standard errors plus floors of 0.006°, 0.008° and 0.012 for quantization and model error. Posterior averages give σ, k and $\Delta_{TM} - \Delta_{TE}$. The indices themselves never enter the fit. Repeating the inference with a uniform kernel of equal variance gives the kernel-shape systematic.

5. Results

5.1 The model reproduces the peak shapes

Across eight wavelength–temperature conditions, the model fits the 48 shape observables with total $\chi^2 = 29$ for 32 degrees of freedom (0.6–9.8 per condition). It reproduces, without tuning, the two systematic TE/TM differences seen in every condition: TE peaks are wider than TM peaks, and the edge reflectance is higher for TE (≈ 0.92 vs ≈ 0.86 at 633 nm). The inferred angular spread is 0.014° (0.24 mrad) at 633 nm, 0.019–0.023° at 532 nm and 0.025° (0.44 mrad) at 964 and 1551 nm. It does not change with temperature, as expected for a property of each laser and its alignment. At 1551 nm the peak shapes also give $\log_{10}$ k = −3.6 ± 1.1, consistent with the literature 1.3×10^{-4} [16].

With these parameters the derivative method underestimates n by 3.5–6.2 × 10^{-4} (0.014–0.025° in θ_c). That is 3–25 times the 0.001–0.005° critical-angle uncertainty usually assumed [7].

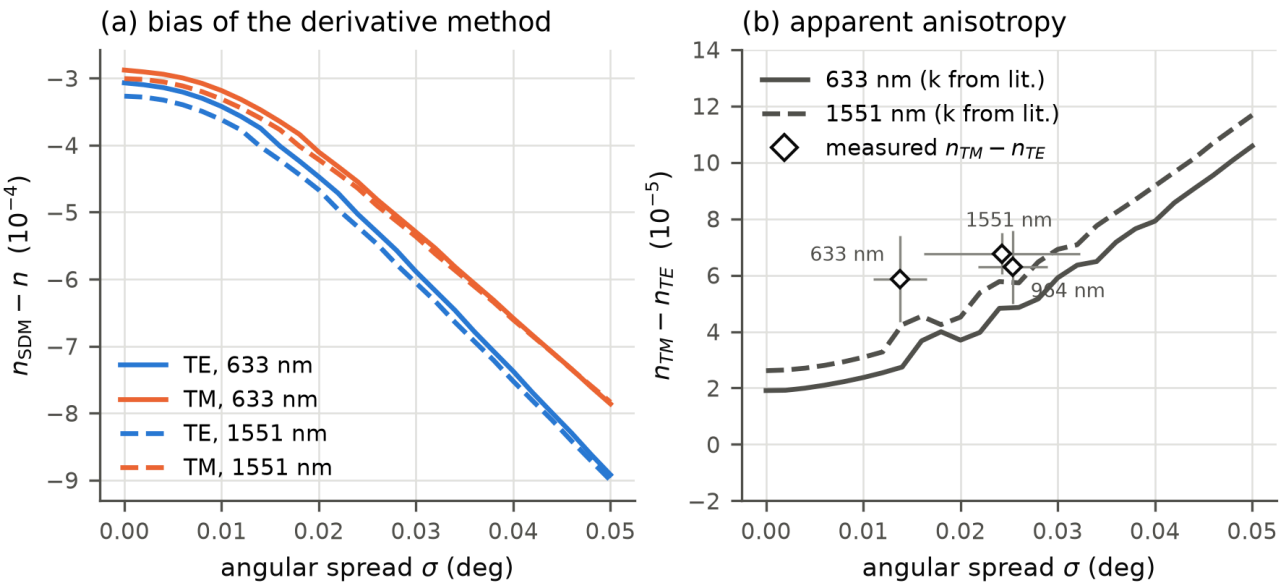


Fig. 3. (a) Simulated derivative-method bias versus angular spread for TE and TM at 633 and 1551 nm. (b) Predicted apparent anisotropy (lines; literature k) and measured $n_{TM} - n_{TE}$ at 25 °C, placed at the σ inferred from peak shapes.

5.2 Predicted versus measured TE/TM difference

At every wavelength the derivative method returns $n_{TM} > n_{TE}$, and the predicted artefact accounts for nearly all of it (Table 1, Fig. 4). The weighted mean over all conditions falls from (6.6 ± 0.6) × 10^{-5} to (−0.04 ± 0.65) × 10^{-5}. The χ^2 is 13.8 for 7 degrees of freedom; scaling the error by 1.40 gives (−0.04 ± 0.91) × 10^{-5}, or $|n_{TM} - n_{TE}| < 1.8 \times 10^{-5}$ at 95 % confidence. Because TE and TM were measured on separate fillings, this bound covers any refill-to-refill offset as well as anisotropy.

λ (nm)	σ (deg)	Measured	Predicted artefact	Corrected
532	0.021	+2.4 ± 6.4	+4.2 ± 0.3	−1.8 ± 6.5
633	0.014	+5.9 ± 1.5	+3.2 ± 0.2	+2.6 ± 1.5
964	0.025	+6.3 ± 1.3	+5.0 ± 0.4	+1.3 ± 1.4
1551	0.024	+6.8 ± 0.7	+8.4 ± 0.5	−1.6 ± 0.9
All 8 conditions (weighted)		+6.6 ± 0.6		−0.04 ± 0.91

Table 1. $n_{TM} - n_{TE}$ in units of 10^{-5} at 25 °C, and the weighted mean over all eight conditions (including 50–80 °C). The predicted artefact uses the posterior k; with the literature k it would be +5.5 at 1551 nm.

The split in Fig. 2b shows what drives the artefact. About +1.9 × 10^{-5} comes from sampling and smoothing alone, at every wavelength; the angular spread adds +0.8 to +3.1 × 10^{-5}; absorption adds +0.7 × 10^{-5}, and only at 1551 nm. Reducing the smoothing window to 5 points does not remove the sampling term, which is set by the 0.0036° angular step. As a partial test, the measured gaps for 9- and 21-point windows follow the model to within about 3 × 10^{-5}.

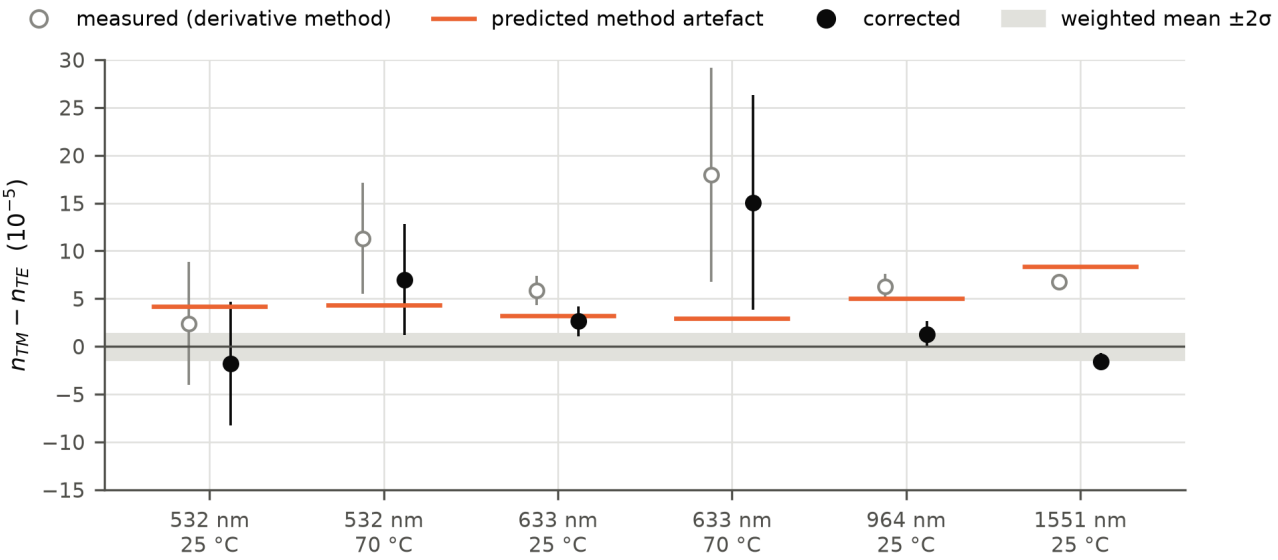


Fig. 4. $n_{TM} - n_{TE}$ per condition: derivative method (open), predicted artefact (bars) and corrected (filled). Grey band: weighted mean ±2σ.

5.3 Consequence for absorption measurements

The TE/TM difference of effective critical angles is the quantity from which polarization-based methods retrieve the extinction coefficient of isotropic media [8]. For water at 1551 nm, an ideal instrument (no angular spread, 0.0005° sampling) gives $n_{TM} - n_{TE} = +0.6 \times 10^{-5}$ from absorption alone. The measured gap is $+6.8 \times 10^{-5}$. Read as absorption, it implies $k = 8.3 \times 10^{-4}$, 6.4 times the true value. Methods that turn small TE/TM or critical-angle differences into k must therefore model the instrument's angular response, or calibrate it on a transparent isotropic sample.

5.4 Rotation direction

Scans taken with the table turning one way read higher than scans taken the other way, by $n_L - n_R = (9.3 \pm 1.8) \times 10^{-4}$ over 12 condition pairs and $(10.4 \pm 0.6) \times 10^{-4}$ at 25 °C (Fig. 5). The offset is the same for TE and TM and stable over half an hour of alternating scans. It corresponds to ±0.019° in θ_c per direction, consistent with a lag between angle encoder and detector reading, or with backlash in the drive. It is ten times the instrument's stated resolution [13]. Averaging the two directions removes it to first order.

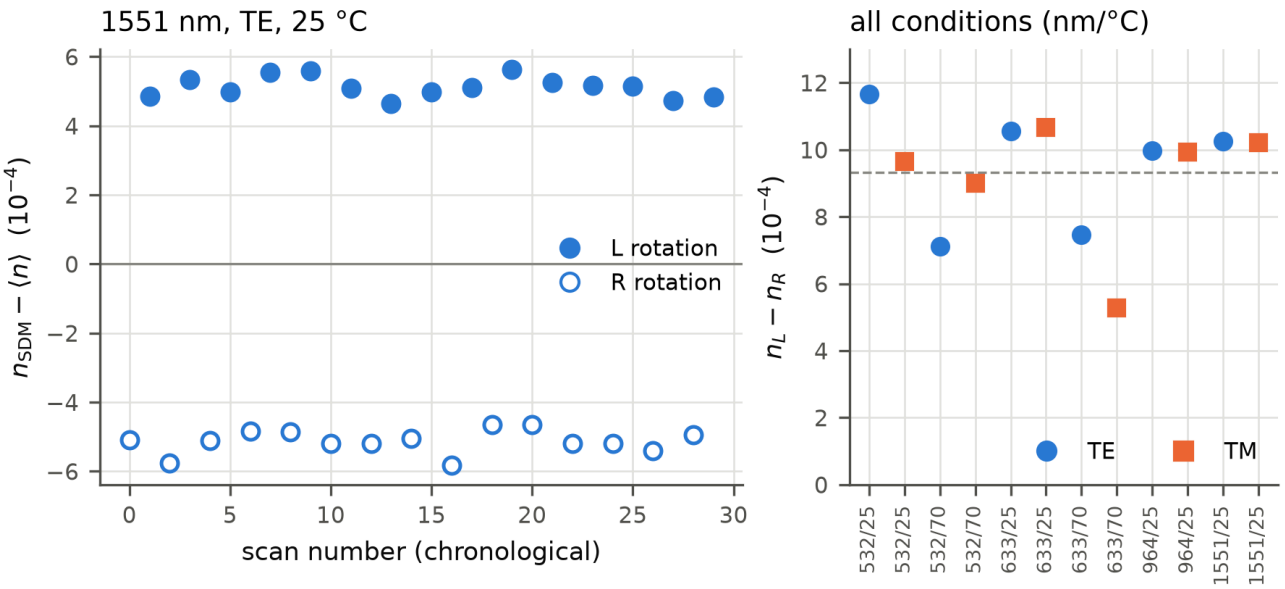


Fig. 5. Left: derivative-method index of 30 consecutive TE scans of water at 1551 nm, relative to their mean; filled = L, open = R rotation. Right: $n_L - n_R$ for every wavelength/temperature (nm/°C) and polarization.

6. Implications, protocol and limitations

The artefact matters wherever a TE/TM index difference below about 10^{-4} is to be measured or interpreted. Examples are stress birefringence in glass, low-birefringence optical polymers, weakly oriented films measured in bulk mode, and liquids. It also affects polarization-based retrieval of k (Section 5.3). For strongly birefringent crystals and drawn polymers ($\Delta n \geq 10^{-3}$) it is negligible.

Calibrating against an index standard in one polarization removes most of the common -3.5 to -6×10^{-4} offset. It does not remove the TE/TM difference, which depends on polarization and on the sample/prism index ratio.

Recommended protocol.

1. Alternate the direction of table rotation and average the two directions.
2. Alternate TE and TM within one filling and one reference, so that refill and re-reference offsets cancel.
3. Record the width, asymmetry and edge reflectance of the derivative peak for each polarization, not only its position.
4. Measure an isotropic reference liquid with a similar n/n_p (water for $n \approx 1.33$). Either infer σ from its peak shapes and apply the model correction, or take its apparent $n_{TM} - n_{TE}$ directly as the instrument's TE/TM offset.
5. Use the finest available angular step; at a fixed step, the smoothing window matters less.

Limitations. The model assumes a symmetric angular response of fixed shape; Gaussian and uniform kernels agree within 0.5×10^{-5}. The corrected anisotropies scatter about 1.4 times more than their uncertainties, suggesting an unmodelled contribution of about 1×10^{-5}. The smoothing-window test agrees only to about 3×10^{-5}. All data come from one instrument, and TE and TM were measured on separate fillings. The strongest remaining test would be a sample of known small birefringence, measured with the protocol above.

7. Conclusions

The derivative method has a polarization-dependent bias that makes isotropic samples appear birefringent by a few 10^{-5}, and its size can be predicted from the measured peak shapes.

1. For water on a high-index prism the artefact is +3 to +8 × 10^{-5} ($n_{TM} > n_{TE}$), measured at 532–1551 nm and reproduced by a forward model with no parameter fitted to the indices. After correction, $|n_{TM} - n_{TE}| < 1.8 \times 10^{-5}$.
2. Angular sampling and an angular spread of only 0.24–0.44 mrad cause most of it; absorption contributes little even at 1551 nm. The usual assumption that beam divergence does not affect θ_c is wrong at the 10^{-4} level.
3. The artefact is proportional to $(n_p/n)^2 - 1$, so it is largest for low-index samples on high-index prisms.
4. Interpreting it as absorption would overestimate water's extinction coefficient at 1551 nm by a factor of 6.4.
5. The direction of table rotation shifts n by ±5 × 10^{-4}, ten times the instrument's stated resolution; averaging both directions removes it.

A calibration measurement on an isotropic liquid, made with the protocol of Section 6, is enough to remove both effects from TE/TM birefringence measurements.

Data, code and credit

A representative sample of the raw scans is provided with this release for verification (`data_sample/`, 16 files: water at 964 and 1551 nm in both polarizations and rotation directions, Intralipid at 1551 nm and cream at 633 nm with their air references). The full dataset (252 water scans, and 115 Intralipid and cream scans with their air references) was recorded at EDML, UNIWA; it may be the property of the laboratory and is not disclosed. The complete analysis code is included (`code/`): it reproduces every number in this paper when run on the full dataset, and processes the sample files individually.

Measurements: Ierotheos Katsoulis, Electronic Devices and Materials Laboratory (EDML), University of West Attica, during an MSc by Research supervised by Prof. Konstantinos Moutzouris. Analysis and text: Ierotheos Katsoulis, 2026.

References

1. S. Singh, "Refractive index measurement and its applications," Phys. Scr. 65, 167–180 (2002). doi:10.1238/Physica.Regular.065a00167
2. G. H. Meeten, A. N. North, F. M. Willmouth, "Errors in critical-angle measurement of refractive index of optically absorbing materials," J. Phys. E: Sci. Instrum. 17, 642–643 (1984). doi:10.1088/0022-3735/17/8/004
3. G. H. Meeten, "Refractive index errors in the critical-angle and the Brewster-angle methods applied to absorbing and heterogeneous materials," Meas. Sci. Technol. 8, 728–733 (1997). doi:10.1088/0957-0233/8/7/006
4. T.-Q. Sun et al., "Scanning focused refractive-index microscopy," Sci. Rep. 4, 5647 (2014). doi:10.1038/srep05647
5. S. Koutsoumpos, P. Giannios, I. Stavrakas, K. Moutzouris, "The derivative method of critical-angle refractometry for attenuating media," J. Opt. 22, 075601 (2020). doi:10.1088/2040-8986/ab8286
6. S. Koutsoumpos, P. Giannios, K. Moutzouris, "Critical angle refractometry for lossy media with a priori known extinction coefficient," Physics 3, 569–578 (2021). doi:10.3390/physics3030036
7. S. Koutsoumpos, P. Giannios, K. Moutzouris, "Two prism critical angle refractometry with attenuating media," Instruments 6, 21 (2022). doi:10.3390/instruments6030021
8. S. Koutsoumpos, P. Giannios, K. Moutzouris, "Critical angle refractometry with optically isotropic attenuating media," Appl. Phys. B 128, 91 (2022). doi:10.1007/s00340-022-07810-1
9. S. Koutsoumpos, P. Giannios, D. Triantis, K. Moutzouris, "Critical-angle differential refractometry of lossy media: a theoretical study and practical design issues," Instruments 3, 36 (2019). doi:10.3390/instruments3030036
10. W. Guo, M. Xia, W. Li, J. Dai, K. Yang, "A two-reflection divergent differentiating critical angle refractometer," Rev. Sci. Instrum. 82, 053108 (2011). doi:10.1063/1.3593501
11. G. Morales-Luna, A. García-Valenzuela, "Viability and fundamental limits of critical-angle refractometry of turbid colloids," Meas. Sci. Technol. 28, 125203 (2017). doi:10.1088/1361-6501/aa8fbe
12. G. Leclerc, A. Yelon, "Birefringence measurements of thin dielectric films by the prism coupler method," Appl. Opt. 23, 2760 (1984). doi:10.1364/AO.23.002760
13. Metricon Corporation, Model 2010/M prism coupler: bulk material and thick-film index/birefringence measurement. metricon.com; application note

14. IAPWS R9-97, "Release on the refractive index of ordinary water substance as a function of wavelength, temperature and pressure" (1997). iapws.org
15. A. H. Harvey, J. S. Gallagher, J. M. H. Levelt Sengers, "Revised formulation for the refractive index of water and steam as a function of wavelength, temperature and density," J. Phys. Chem. Ref. Data 27, 761–774 (1998). doi:10.1063/1.556029
16. D. J. Segelstein, "The complex refractive index of water," M.S. thesis, University of Missouri–Kansas City (1981).
17. G. M. Hale, M. R. Querry, "Optical constants of water in the 200-nm to 200-μm wavelength region," Appl. Opt. 12, 555–563 (1973). doi:10.1364/AO.12.000555
18. M. Born, E. Wolf, Principles of Optics, 7th ed. (Cambridge University Press, 1999).
19. A. Savitzky, M. J. E. Golay, "Smoothing and differentiation of data by simplified least squares procedures," Anal. Chem. 36, 1627–1639 (1964). doi:10.1021/ac60214a047
20. B. R. Horowitz, T. Tamir, "Lateral displacement of a light beam at a dielectric interface," J. Opt. Soc. Am. 61, 586 (1971). doi:10.1364/JOSA.61.000586